OSMOTIC FRAGILITY MODEL FOR RED CELL POPULATIONS

H. A. MASSALDI, G. V. RICHIERI, AND H. C. MEL

*Department of Biophysics and Medical Physics and Lawrence Berkeley Laboratory,
University of California, Berkeley, California 94720*

ABSTRACT A model that predicts the osmotic fragility curve of a red cell population is developed by relating the critical osmotic pressure to the size distribution of the cells, determined by resistive pulse spectroscopy. Two of the parameters involved, namely the normalized osmotic volume correction, B, and the swelling index, k, are previously determined from the experimental average properties of the population. From these values the critical volume of the cell is obtained, and is shown to be 6–12% larger than the first spherical volume, obtained from an independent experiment. A new parameter, n, a measure of the surface area distribution of the cells, is incorporated through a simple function that relates the critical volume to the size of the cells, and is theoretically shown to be linked to parameters k and B. The model is used to fit and interpret fragility data obtained in this laboratory for normal and sickle cell samples. From the values of n obtained for normal samples, the model predicts an essentially constant surface-to-volume ratio within an individual's cell population. For sickle cell samples, instead, the value of index n is negative, thereby supporting an increase in excess surface area as cell size decreases. Both findings are in agreement with direct observations reported in the literature. It is concluded that this set of parameters may be used to develop an index classification of blood disorders.

INTRODUCTION

The main value of the osmotic fragility test, as commonly used in clinical practice, is to confirm important morphological abnormalities of a blood sample, such as the presence of leptocytes and spherocytes (1). However, the osmotic fragility of red cells not only reflects the peculiarities in average membrane and cytoplasmic properties of a given sample, but it can also provide information about the distribution of those properties within the sample itself. Thus, by use of density-fractionation techniques, several authors (2–4) have been able to correlate differences in cell density and osmotic fragility with the relative age of the erythrocytes in terms of "young," "mature," and "old" cells. Although this association has been questioned (5), it seems that more precise fractionations should confirm those results (6).

A more systematic and quantitative classification of normal and pathological red blood cells may be obtained by developing a model that relates the osmotic properties of a given blood cell sample with the morphological characteristics of its distribution. A population of normal red blood cells can be represented by a frequency-size distribution curve for apparent cell volume, which can readily be obtained by resistive pulse spectroscopy (RPS) (7, 8).

When the external osmotic pressure is reduced arbitrarily, the cell volume increases according to a relationship which deviates, to a greater or lesser extent, from ideal behavior. In particular, at the onset of hemolysis, a distribution of critical volumes associated with the distribution of critical osmotic pressures can be expected to hold.

A classical osmotic pressure-cell volume relationship was proposed by Ponder (9) through a well-known empirical equation that includes his parameter, R. An equivalent form of this equation was used by Canham (10) to obtain semitheoretical fragility curves which adequately reproduced the experimental data, obtained by the classical method of hemoglobin release. However, the procedure required the estimation of the hemolytic volume by means of microscopic determinations of surface area for a statistically significant number of cells, a method that is not practical for general application.

In this paper, we present a model that relates the fragility curve of a given red cell population to the cumulative frequency-size distribution for the same blood sample, both determined by the RPS technique. A simple expression for the critical hemolytic volume as a function of cell size is used to link the critical volume of each cell to the corresponding osmotic pressure. In this way, a distribution of "critical" osmotic pressures, which gives rise to the fragility curve, is predicted. The model is used to simulate, fit, and interpret osmotic fragility data obtained in this laboratory for different samples of normal and sickle red blood cells. The parameters estimated for either type of

blood are used to infer the respective surface area distribution characteristics in quantitative terms.

MODEL

The basic volume-osmotic pressure relationship for a red cell which contains a portion of its volume, b, osmotically inactive is (11, 12)[1]

$$\frac{\Pi}{\Pi_{iso}} = \frac{V_{iso} - b}{V - b}.$$ (1)

If we wish to consider for any individual cell, i, the critical osmotic pressure, $\Pi_{c,i}$, corresponding to its critical volume, $V_{c,i}$, Eq. 1 can be rewritten in the form

$$\Pi_{c,i}^* = \frac{\Pi_{c,i}}{\Pi_{iso}} = \frac{V_{iso,i} - b_i}{V_{c,i} - b_i}.$$ (2)

To proceed further towards our goal of directly linking volume distribution information with fragility distributions, we need a means of expressing, for any given cell, the b_i and $V_{c,i}$ in Eq. 2 as a function of the cell's volume.

The Parameter b

As the osmotically inactive volume of the cell, this parameter may be associated with the cell's hemoglobin content. Qualitatively, from cohort labeling and cell fractionation experiments, one can conclude that the ratio $B = b_i/V_{iso,i}$ is larger for smaller and older cells in the population (14, 15). The extent of the cell's "shrinkage" (relative dehydration) can be estimated from the MCHC value for the smaller, denser, more spherical, "bottom," fractions. It is ~40%, whereas the overall population average is ~33% (6). This 40/33 = 21% increase corresponds quite closely to the approximate 20% figure for the relative volume decrement (from the median volume) of the lower portion of a typical size distribution curve (16). Therefore, the simplest qualitative relationship we can write for b_i to reflect this correspondence is

$$b_i \approx \text{constant} = b,$$ (3)

which assumes that the hemoglobin content is approximately the same for the cells in a given population.[2]

---

[1]Eq. 1 is mathematically equivalent to the classical equation of Ponder for a population of cells (9): $V/V_{iso} = RW (\Pi_{iso}/\Pi - 1) + 1$, where $RW = 1 - b/V_{iso}$, is the osmotically active fraction of cell volume, V. (The parameter W is the isotonic volume fraction of water, and R measures the relative ideality of the system on a scale of 0 to 1). Freedman and Hoffman (13) have shown that this equation can be also obtained from their physicochemical equilibrium model by assuming a constant total osmotic coefficient for the cell interior.

[2]This approximation holds for a value of b averaged over each group of cells of the same age. Within this group, there may be differences in the specific Hb contents of each cell, due to differences in the size of reticulocytes at birth.

The Ratio $V_{c,i}/V_{iso,i}$

In principle, the association between this ratio, sometimes called the "swelling ratio" (4), and the cell size within the distribution may be either positive or negative. For a population of normal cells, from the same kind of fractionation experiments referred to previously, we know that this ratio is smaller for the smaller-sized cells in the population. This is so because the isotonic volume for the smaller cells is closer to sphericity than that for the larger cells (2, 4, 6, 14, 15).

The simplest monotonic functional relationship between the swelling ratio and the isotonic volume is a direct proportionality, $V_{c,i}/V_{iso,i} \propto V_{iso,i}$. The proportionality coefficient is conveniently expressed as a dimensionless constant, k, divided by the median isotonic volume for the population, $\hat{V}_{iso}$, and we can write

$$\frac{V_{c,i}}{V_{iso,i}} = k\frac{V_{iso,i}}{\hat{V}_{iso}}.$$ (4)

Clearly, the constant k represents the swelling ratio for the median volume cell: $k = \hat{V}_c/\hat{V}_{iso}$, and is called the "swelling index" of the population. Because there is no "a priori" reason to assume that a restricted relationship like Eq. 4 should hold quantitatively, for the purposes of this model and for fitting the experimental data we generalize this equation to the form

$$\frac{V_{c,i}}{V_{iso,i}} = k\left(\frac{V_{iso,i}}{\hat{V}_{iso}}\right)^n$$ (5)

or alternatively,

$$V_{c,i} = k V_{iso,i}\left(\frac{V_{iso,i}}{\hat{V}_{iso}}\right)^n = \hat{V}_c\left(\frac{V_{iso,i}}{\hat{V}_{iso}}\right)^{n+1},$$ (6)

where n is an adjustable parameter. Also in this way, abnormal blood cell samples that depict a relationship inverse to that expressed by Eq. 4 may be allowed consideration, in which case a negative value of n should be expected in Eq. 6.

Introducing relations 3 and 6 into Eq. 2 yields

$$\Pi_{c,i}^* = \frac{V_{iso,i} - b}{\hat{V}_c\left(\frac{V_{iso,i}}{\hat{V}_{iso}}\right)^{n+1} - b}.$$ (7)

For purposes of comparing different populations, it is convenient to express Eq. 7 in the normalized, dimensionless form obtained by dividing its numerator and denominator by $\hat{V}_{iso}$.

$$\Pi_{c,i}^* = \frac{V_i^* - B}{k(V_i^*)^{n+1} - B},$$ (8)

where $B = b/\hat{V}_{iso}$ and $V_i^* = V_{iso,i}/\hat{V}_{iso}$. Eqs. 7 or 8 thus represents the population equation corresponding to the elementary Eq. 2, applied to the critical state.

Limiting Values and Parameters for Normal Blood Cells

It is interesting to consider the range of values that $II^*_{c,i}$ can theoretically achieve for normal red cell samples with V^*_i is varied between virtual, numerical limits. Thus, from Eq. 8, for V^*_i tending to a very large value, $II^*_{c,i}$ goes to zero, which represents the lower osmolality limit for a cell with the highest swelling ratio. For very small values of V^*_i, on the other hand, Eq. 8 indicates that $II^*_{c,i}$ tends to unity, which would correspond to the upper osmolality limit for a cell with the lowest swelling ratio. In this case, however, there exists a previous physical limit, imposed by the model on the lower values of V^*_i. This is given by $V^*_i = B$, because the normalized cell volume cannot be smaller than the nonosmotic volume fraction, represented by parameter B. Also because of this, the corresponding swelling ratio, $V_{c,i}/V_{iso,i}$ is equal to unity, because there is no "osmotic" liquid available to induce the swelling of the cell. Therefore, Eq. 5 is, in this limit,

$$\frac{V_{c,i}}{V_{iso,i}} = k(V^*_i)^n = k(B)^n = 1, \tag{9}$$

which leads to the following relationship.

$$n_e = -\log k/\log B, \tag{10}$$

where the subscript e in parameter n means that this is a theoretical, or "expected," value. According to Eq. 9, the limit of $II^*_{c,i}$ for $V^*_i = B$ in Eq. 8, is undetermined. The value of $II^*_{c,i}$ corresponding to this limit can be found by applying the L'Hopital rule to Eq. 8, with the result,

$$II^*_{c,i}|_{V^*_i=B} = II^*_B = \frac{1}{1 + n_e} \tag{11}$$

Eqs. 10 and 11 represent an important finding of the present model, because they provide a theoretical linkage between the relevant parameters, and put a physical limit to the higher critical osmolalities that can be observed for a given normal blood sample.

Distribution of Excess Surface Areas

Another consequence of the present model is that, by proper determination of the set of parameters, it would be possible to obtain an estimate of the surface area distribution of the sample. In effect, by applying the surface area–volume relationship for the sphere to the critical median volume and to a variable cell size, one obtains

$$\frac{V_{c,i}}{V_c} = \left(\frac{A_i}{\bar{A}}\right)^{3/2}. \tag{12}$$

On the other hand, from Eq. 6 above,

$$\frac{V_{c,i}}{\bar{V}_c} = \left(\frac{V_{iso,i}}{\hat{V}_{iso}}\right)^{n+1} \tag{13}$$

and from Eqs. 12 and 13,

$$\frac{A_i}{\bar{A}} = \left(\frac{V_{iso,i}}{\hat{V}_{iso}}\right)^{2(n+1)/3}, \tag{14}$$

which indicates that the distribution of excess surface areas can be determined from the size distribution and the value of parameter n.

METHODS

Sample Preparation and Procedure

Blood samples were obtained by finger prick from 11 healthy donors (mean age 32 yr; range, 21–54 yr) and from three patients (mean age, 21 yr; range, 7–26 yr) with homozygous sickle cell disease. Diagnosis was made by demonstrating only the presence of Hb S by electrophoresis, with a variable amount of Hb F. The patients had not received transfusions within the previous 14 wk. Two or three drops of blood were immediately diluted 1:100 into Dulbeccos's phosphate-buffered saline (PBS, in g/liter: NaCl, 8.0; KCl, 0.2; Na_2HPO_4, 1.15; KH_2PO_4, 0.2; $MgCl_2.6H_2O$, 0.1. Slight adjustments were made to 300 mOsm at pH 7.4, by adding small amounts of NaCl, water, NaOH, and KCl, as appropriate). The cells were allowed to equilibrate with the stock solution for 30–60 min at room temperature before performing the tests. Within 5 s before the RPS measurements, a secondary dilution, 2:100, was further carried out. Solutions of different osmolalities were prepared by diluting the original PBS solution with deionized water. The final osmolality was measured with a freezing point, Fiske Osmometer, model G-62 (Fiske Assoc., Inc., Uxbridge, MA).

RPS Measurements

The details of the electronics and computer operation of the RPS technique are described elsewhere (8, 16). The correction of the cell volume for shape factor has been recently analyzed and evaluated (17). The same procedure has been applied to the data used here, so that our reported values of average cell volume are the true values obtained after the correction. The distributed cell volumes within each sample were corrected for differences in shape factor by the following procedure. The distribution was first determined without the correction. Then, from the fitting of experimental fragility data, as described below, parameter n was estimated, and a given swelling ratio could be assigned to each volume through Eq. 5. From Fig. 2 of Richieri et al. (17), the shape factor for each individual cell volume was estimated (oblate assumption), and the whole size distribution curve was recalculated. Only one iteration was needed because the maximum correction effect was found to be <3% in all cases.
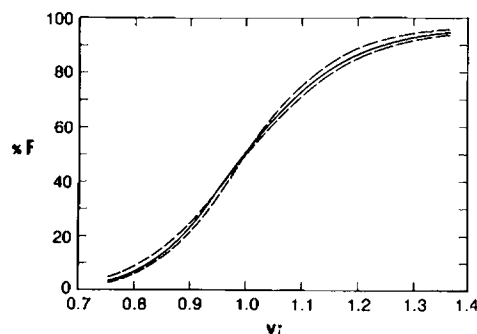

FIGURE 1 Limiting range (dashed) and average (solid) curves of percent cumulative frequency, %F, of normalized size distributions for 10 normal blood samples, determined by RPS.

RPS osmotic fragility data were obtained by sizing the sample at 25°C and different PBS osmolalities, and selecting those in the range which gave rise to different degrees of hemolysis, as assessed by the fraction number of ghosts produced (18). The fragility data were then plotted as percent ghosts (%G) produced vs. PBS osmolality. Akeson and Mel (18) have demonstrated the equivalence of this technique with respect to the classical method of hemoglobin release.

Calculation Procedure: Simulated Osmotic Fragility Curves

Theoretical osmotic fragility curves were obtained from Eq. 8 for the case $n > 0$ (positive association of swelling ratio and cell size). First, for a given set of values of the parameters (k, B, n), the values of $II^*_{c,i}$ were calculated as a function of the normalized cell volume taken from the average size distribution given in Fig. 1. Then, by considering that cells smaller than each volume V^*_i have already hemolyzed, the percent cumulative frequency (%F) of cell sizes up to V^*_i, associated with $II^*_{c,i}$, was directly taken to be the percent ghosts (%G) produced. In this way, simulated RPS fragility curves, %G vs. $II^*_{c,i}$ (or $II_{c,i}$), were obtained from the size distribution and use of Eq. 8.

Osmotic Fragility Parameters and Fitting Procedure

To fit osmotic fragility data according to Eq. 8, it was first necessary to determine the average population parameters, B and k. The volume correction parameter, B, for a given sample was determined from the results of an osmotic swelling experiment. For this purpose, Eq. 1 was written explicitly for the median volume as

$$\frac{\hat{V}}{\hat{V}_{iso}} = \frac{II_{iso}}{II}(1 - B) + B. \quad (15)$$

The sample was subjected to different hypotonic, nonhemolytic osmolalities of PBS, and a plot was made of $\hat{V}$ vs. $1/II$, which rendered a straight line, as shown in Fig. 2 for sample No. 1H. A direct reading on the plot yielded the values of the isotonic cell volume, $\hat{V}_{iso}$ and the first spherical volume, $\hat{V}_s$, as indicated. From the slope of the line: $II_{iso}(1 - B)\hat{V}_{iso}$ (Osm.μ^3), the value of B was estimated.

For the calculation of the swelling index, k, the value $V^*_i - 1$ was substituted into Eq. 8, which then reads

$$II^*_c = \frac{1 - B}{k - B}. \quad (16)$$

In this equation, the constant II^*_c is the critical relative osmolarity for the median of the population of cells, associated with the 50% fragility value of the sample. From Eq. 16,

$$k = \frac{1 - B(1 - II^*_c)}{II^*_c} \quad (17)$$

was calculated by substituting the value of B, estimated as indicated above, and the value of $II^*_c - II(50\%G)/II_{iso}$. $II(50\%G)$ was determined from the experimental fragility data for the same sample, by direct interpolation of the osmolality at 50% ghosts produced. With these values of B and k, and the volumes from the specific size distributions given in Figs. 3 and 4, the corresponding experimental fragility data were fitted by graphical iteration with the value of n in Eq. 8, as follows.

The 50% fragility point ($II\{50\%G\}$) was first located and assigned to $V^*_i - 1$. Other values of V^*_i, above and below one, were then used to obtain the corresponding $II_{c,i}$ from Eq. 8. For normal blood samples, the percent ghosts (%G) associated with the $II_{c,i}$ values were directly taken to be the percent cumulative frequency (%F) below V^*_i in Fig. 3. For sickle cells instead the %G produced was calculated as the percent frequency above V^*_i, that is, (100 − %F) in Fig. 4, because in this case the smallest cells have the largest surface-to-volume ratio (19) and therefore can be expected to be the more resistant osmotically. Absolute values of n between 0 and 1 were tentatively assumed. (For normal samples the expected n_e value provides a good initial estimate.) Then by using values of V^*_i of 0.8 and 1.2, the adequacy of the chosen n value was assessed and corrected by trial and error until a satisfactory fit, as judged visually, was obtained for these points. The other V^*_i values were then used to cover the full range of data. In this way, a set of experimental values of the osmotic fragility parameters B, k, and n were obtained for each sample.

RESULTS

Fig. 1 shows the envelope of cumulative relative size distributions, %F vs. V^*_i, of blood samples obtained from 10 healthy donors, as determined by the RPS technique. In this figure, the two limiting broken lines correspond to the range of the size-distribution data, with average values represented by the full continuous line. It can be also noted that, when plotted in this normalized fashion, all curves go
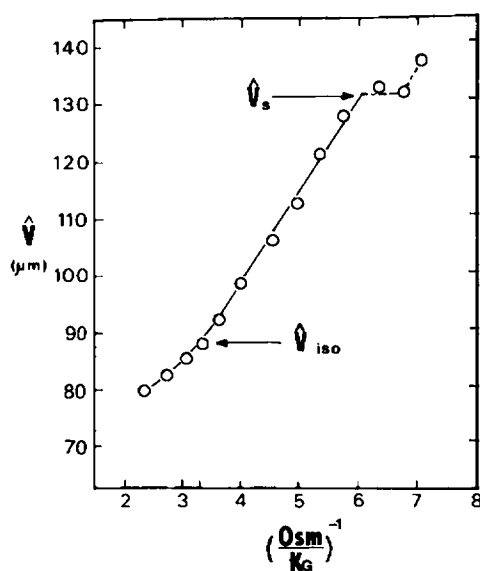

FIGURE 2 Volume change as a function of osmotic pressure for sample No. 1H, determined by RPS at 25°C. Arrows indicate the median values of the isotonic volume, $\hat{V}_{iso}$, and the first spherical volume, $\hat{V}_s$.
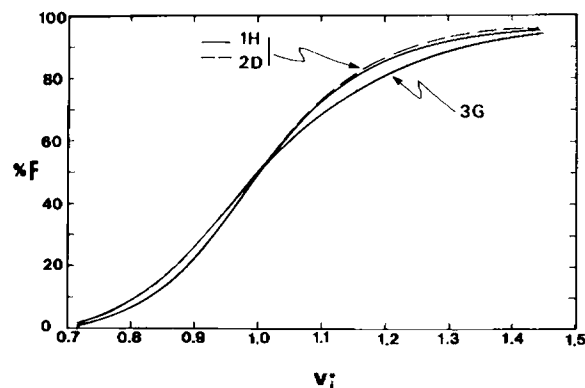

FIGURE 3 Cumulative frequency of normalized size distribution for red blood cell samples from three healthy donors, two of which (Nos. 1H and 2D) are represented in Fig. 1.
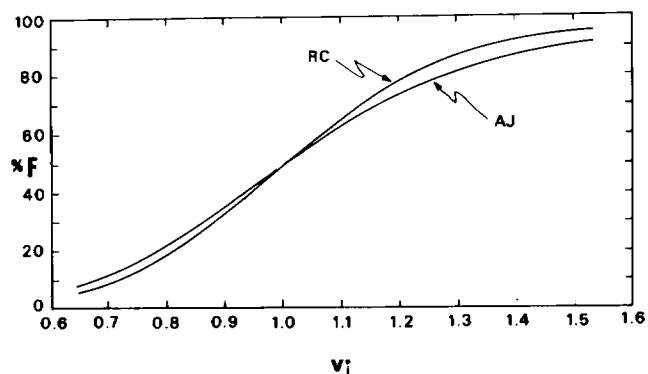
FIGURE 4 Cumulative frequency of normalized size distribution for sickle (HbSS) red blood cell samples from two patients.
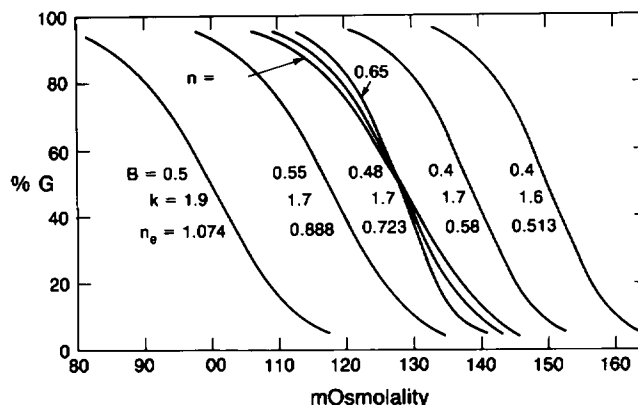

FIGURE 5 Simulation of population fragility curves, % ghosts vs. osmotic pressure, for a practical range of parameter values, according to the present model. See text for discussion.

through the point of 50% frequency and $V_i^* = 1$. Thus, the average curve provided representative size distribution values to be used in the simulation experiments.

Fig. 3 shows the size distributions corresponding to two of the donors represented in Fig. 1, and an extra one, whose distribution falls outside the range shown in that previous figure. The cell size distributions of the blood samples from two of the three HbSS donors are plotted in Fig. 4. Percent ISC (irreversible sickle cells) for these patients were (mean ± SD): AJ, 14 ± 8; RC, 9 ± 6. Table I lists several parameters of location of the cell size distributions shown in Figs. 3 and 4.

Fig. 5 shows fragility curves for normal blood, simulated according to the procedure described above (see Methods) and by using the average size distribution shown in Fig. 1. It can be observed that, for increasing values of the swelling index, k, or the volume correction parameter, B, the curves are shifted to the left, i.e., to the region of less fragile populations. The values of the "expected" parameter, n_e, calculated from Eq. 10, are also indicated in Fig. 5 for each curve. For the curve with $B = 0.48$, the effect of using values of n above and below n_e is shown to change only the slope of the curve, and not to affect the location of the 50% fragility point.

Table II lists the characteristic values and parameters obtained from the RPS size distribution in the osmotic swelling experiments, for the samples of Figs. 3 and 4. Included are the median critical volume, $\hat{V}_c$, obtained from

the values of k and $\hat{V}_{iso}$, the median first spherical volume, $\hat{V}_s$, determined from the plot of Fig. 2 as already described, and the percent difference between them. Also listed are the "measured" values of n, obtained from the fitting procedure for these samples, and the expected values, n_e, for the normal cell samples.

Fig. 6 shows five sets of RPS fragility data, three of which belong to the healthy donor samples whose size distributions are shown in Fig. 3. The remaining two sets of data correspond to the HbSS blood samples from donors with sickle cell disease, which have the size distributions given in Fig. 4. The solid lines in Fig. 6 are the result of fitting the data with Eq. 8, by using the parameters listed in Table II and the corresponding size distributions, as described earlier. The only adjustable parameter is the index n, whose experimental values are also listed in Table II.

DISCUSSION

An essential feature of the present model is the use of relative size distributions of the cell population as the basic factor which determines the distribution of osmotic fragilities. Figs. 1, 3, and 4 show the differences and similar patterns of various distributions around the median value. In all cases, the spread of the distribution is larger for values $V_i^* > 1$, than for those at $V_i^* < 1$, reflecting some degree of skewness to the right of the frequency distribution. Comparison of Figs. 1 and 3 indicates that, although a tight representation of the data is possible in this normalized form, a distinct variability among individuals should be expected, as is shown by the sample No. 3G in Fig. 3, and also by data from other samples, not shown. Fig. 4 also shows that the size distribution of sickle cell samples follows similar patterns, although clearly, wider distributions are apparent in this case.

The trend of the simulated fragility curves in Fig. 5, for increasing values of the index k, is in accordance with the physical expectation that a larger prehemolytic swelling

TABLE I

MEASURES OF LOCATION (IN ARBITRARY UNITS) AND COEFFICIENT OF VARIATION FOR THE SIZE DISTRIBUTION OF RED CELL SAMPLES SHOWN IN FIGS. 3 AND 4

Sample	Blood type	$\hat{V}$ (modal)	$\hat{V}$ (median)	V (mean)	CV
1H	Normal	30.22	30.67	31.38	0.139
2G	Normal	29.36	30.20	31.08	0.162
3D	Normal	32.73	32.97	33.88	0.139
4AJ	Sickle	28.65	29.91	31.73	0.289
5RC	Sickle	29.07	29.15	29.83	0.222

TABLE II

CHARACTERISTIC VALUES AND PARAMETERS OF OSMOTIC SWELLING AND FRAGILITY OF THE RED CELL POPULATIONS DESCRIBED IN TABLE I

Sample	Blood type	$\hat{V}_{iso}$	$\hat{V}_i$	II (50% G)	B	k	$\hat{V}_c$	$\dfrac{\hat{V}_c - \hat{V}_i}{\hat{V}_i}$	n	n_e
		μ^3	μ^3	mosm			μ^3	%		
1H	Normal	87.2	130.0	136.5	0.432	1.680	146.5	12.7	0.618	0.618
2G	Normal	85.1	128.9	128.0	0.491	1.683	143.2	11.0	0.630	0.732
3D	Normal	95.2	148.3	127.0	0.467	1.727	164.4	10.9	0.650	0.718
4AJ	Sickle	85.7	155.6	96.5	0.561	1.924	164.9	6.0	−0.15	—
5RC	Sickle	87.5	167.6	100.0	0.478	2.046	179.0	6.8	−0.15	—

capacity corresponds to a more osmotically resistant (less fragile) population of cells. Along the same line of reasoning, a larger B value (higher fraction of nonliquid volume) at constant k implies that the population has a higher ratio of surface area to liquid volume, again allowing an increased swelling capacity, and thereby increased resistance, before hemolysis. The slope of the curves decreases slightly in going from right to left in Fig. 5, that is, for larger k or B values. For a given set of these values, however, the slope is clearly sensitive to changes in the value of n, larger values giving lower slopes, as indicated for the set $B = 0.48$; $k = 1.70$.

The good fitting of experimental fragility data from healthy subjects in Fig. 6 (the three solid curves on the right) indicates that the present model provides an adequate representation of cell population fragility. The values of k obtained, approximately between 1.68 and 1.73, are in the expected range for the swelling capacity of erythrocytes. It is somewhat higher than one reported value of the swelling index for nonfractionated cell samples, 1.62 (4). If instead, the normalized first spherical volume $\hat{V}_i/\hat{V}_{iso}$, is calculated, lower values, between 1.490 and 1.558, are found. As indicated in Table II, this reflects the 10–13% larger values encountered for $\hat{V}_c$ with respect to $\hat{V}_i$, as determined here. This figure is somewhat higher than the

FIGURE 6   Experimental osmotic fragility data for normal (*open points*) and sickle (*solid* points) cell samples which have the size distributions shown in Figs. 3 and 4. The lines are the result of fitting the data with the indicated values of the parameters, according to the present model. Values within parentheses for the three normal samples (on the right) are the corresponding expected n value, n_e.

relative volume increase of ~8%, to be expected from the surface area expansion during the stress stage of osmotic hemolysis (20). On the other hand, the values of B listed in Table II, somewhat below 0.5, are also within the reasonable expectation, and in good harmony with reported values from the literature (4, 21, 22).

In Fig. 6, two features of the fitted fragility curves for healthy subjects are particularly interesting. First, the two osmotic fragility curves that appear almost superimposed correspond to the two different size distributions shown in Fig. 3 (samples 3D and 2G), whereas the parallel, separate fragility curve shown on the right (1H) has practically the same size distribution as sample 2G. This suggests that there is no correlation between the osmotic properties and the characteristics of the size distribution and provides good support for the use of the present model for fitting purposes. Secondly, it can be observed that the slopes of the curves have been adjusted with values of n close to n_e, and in one case (1H), with precisely the same value. We interpret this result as strongly supporting Eq. 6 as an appropriate expression for the distribution of critical volumes. It also suggests that the value of n_e, given by Eq. 10 for normal blood, represents a true physical expectation, rather than merely a mathematical entity.

The osmotic fragility data for the sickle cell samples (4AJ and 5RC) shown in Fig. 6 were also reasonably fit by Eq. 8, with the values of B, k, and n shown in Table II, and the corresponding size distributions of Fig. 4. The values of B for this case are also within the range expected for normal cells, but those for the swelling index, k, are higher than those for normal samples. This would indicate that the increased osmotic resistance observed for the sickle cell population is mainly the consequence of a larger swelling capacity. However, the effect of a somewhat higher B value, which renders a lower slope (lower R) in Ponder's equation, may be also contributing to the increased resistance for sample 4AJ. The fitted n values are negative, indicating an inverse dependence of the swelling ratio with cell size in Eq. 6. For this reason, the limiting values and relationships given by Eqs. 9–11, developed for normal cells, do not hold now. The absolute value of n, on the other hand, is relatively small. This suggests that, according to the present model, the lower slope displayed by the fragility
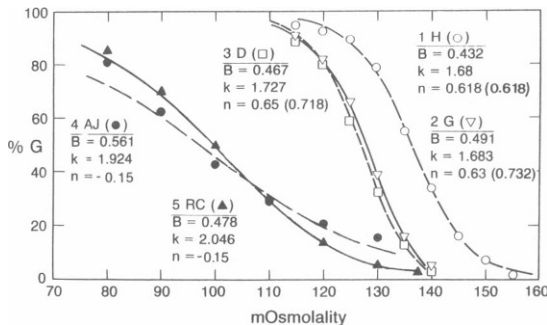
data of sickle cell samples is mainly the consequence of the wider distribution of cell sizes (Fig. 4), whereas the effect of the excess surface area distribution (measured by n) seems to be less important.

Results for other types of cell samples may be readily interpreted with the present model. Thus, the increased osmotic fragility of red cells in spherocytosis can be clearly ascribed to a larger cell volume at isotonicity, which would reduce both the swelling index k, and probably the volume correction parameter B as well, thereby shifting the fragility curve to the right in Fig. 5. On the other hand, recently reported decreased fragility of normal red cells treated at 40°C (23) can be interpreted through a larger value of the swelling index k. In this case, it can be shown that this is due to both a reduced isotonic volume (23) and to a critical volume somewhat larger than the values reported in Table II for 25°C. This results in a temporary augmentation of the membrane surface area in the order of 9% (23, 24), beyond the value of 4–6% that can be normally expected at 25°C (20, 23, 24). In this case, parameter B does not seem to play a role, however, because the slopes of the lines at the different temperatures (0–40°C) are essentially the same (24).

Now, on the basis of the experimental values of n, it is possible to ascertain how the excess surface area distribution looks like for each type of cell population. Thus, for normal cells, by considering $n = 0.63$ a value representative of those in Table II, we have, from Eq. 14,

$$\frac{A_i}{\bar{A}} = \left(\frac{V_{iso,i}}{\bar{V}_{iso}}\right)^{1.087},$$ (18)

or

$$\frac{A_i}{\bar{A}} \simeq \frac{V_{iso,i}}{\bar{V}_{iso}}.$$ (19)

That is, the distribution of surface areas follows closely that for the cell volumes. Eq. 19, written in the form

$$\frac{A_i}{V_{iso,i}} \simeq \frac{\bar{A}}{\bar{V}_{iso}},$$ (20)

also implies that the surface-to-volume ratio of normal red blood cells of a given population is essentially a constant. This finding of the present model is supported by experimental results from the literature (4), where a constant ratio A/V has been reported for different fractions of normal red cells. It may be speculated that Eq. 20 represents a conservation of the transport capacity of the cell during cell life. General solutions for the kinetics of osmotic swelling (20, 25, 26) or glucose uptake in the red cell (27) show that the flux of mass is proportional to this ratio. The constancy of the surface-to-volume ratio would therefore suggest that, in a transient process, the equilibration times of individual cells are independent of the particular cell age.

For the sickle cell samples, with the value of $n = -0.15$ (Table II) in Eq. 14, one obtains

$$\frac{A_i}{\bar{A}} = \left(\frac{V_{iso,i}}{\bar{V}_{iso}}\right)^{0.57}.$$ (21)

Therefore, the distribution of surface area of sickle cells is narrower than the corresponding size distribution, in contrast with the result obtained for normal cells. At the same time, however, and because of this, a significant variation of the surface-to-volume ratio within a given sample is the likely expectation in this case. Also the less-than-one exponent in Eq. 21 indicates that smaller cells will have an increased surface area, in accordance with the observations of Nash et al. (19) for fractionated sickle cells. In this respect, it is possible that the presence of a subpopulation of smaller, dehydrated cells such as the ISCs, which have lost relatively more volume than area, is partly responsible for the modified patterns of size and fragility distribution of sickle cells with respect to those of the normal ones.

CONCLUSIONS

The model developed here seems to perform well for quantitatively describing and interpreting the osmotic fragility behavior of different types of blood samples. By proper use of the RPS technique, both the size and fragility distributions, and the average osmotic properties of a given sample, can be determined in a straightforward manner. By incorporating this information in the present model, the value of the parameter set, characteristic of each sample, can be readily obtained. The systematic application of this procedure to a sufficient number of diverse red blood cell types, may allow the development of a new index classification of blood disorders.

REFERENCES

1. Wintrobe, M. M. 1974. Clinical Hematology, Lea and Febiger, Philadelphia. 774–775.
2. Bessis, M. A. 1973. Living Blood Cells and their Ultrastructure. Ch. 2. Springer-Verlag, Berlin.
3. Bocci, V. 1981. Determinants of erythrocyte ageing: a reappraisal. *Br. J. Haematol.* 48:515–522.
4. Linderkamp, D., and H. J. Meiselman. 1982. Geometric, osmotic and membrane mechanical properties of density-separated human red cells. *Blood.* 59:1121–1127.
5. Rifkind, J. M., K. Araki, and E. C. Hadley. 1983. The relationship between the osmotic fragility of human erythrocytes and cell age. *Arch. Biochem. Biophys.* 222:582–589.
6. Clark, M. R., and S. B. Shohet. 1985. Red cell senescence. *Clin. Haematol.* 14:223–257.
7. Mel, H. C., and J. P. Yee. 1975. Erythrocyte size and deformability studies by resistive pulse spectroscopy. *Blood Cells (Berl.)* 1:391–399.
8. Yee, J. P., and H. C. Mel. 1978. Cell membrane and rheological mechanisms: dynamic osmotic hemolysis of human erythrocytes

and repair of ghosts, as studied by resistive pulse spectroscopy. *Biorheology.* 15:321–339.

9. Ponder, E. 1948. Hemolysis and Related Phenomena. Ch. 3. Grune & Stratton Inc., New York.

10. Canham, R. 1970. Curves of osmotic fragility calculated from the isotonic areas and volumes of individual human erythrocytes. *Cell Physiol.* 74:203–212.

11. Dick, D. A. T. 1966. Cell Water. Ch. 4. Butterworths, Washington, DC.

12. Macey, R. I. 1978. Membrane Transport in Biology. Ch. 1. G. Giebisch, D. C. Tosteson, and H. H. Ussing, editors. Springer-Verlag, Berlin.

13. Freedman, J. C., and J. Hoffman. 1979. Ionic and osmotic equilibria of human red blood cells treated with nystatin. *J. Gen. Physiol.* 74:157–185.

14. Chalfin, D. 1956. Difference between young and mature rabbit erythrocytes. *J. Cell. Comp. Physiol.* 47:215–239.

15. Marks, P. A., and A. B. Johnson. 1958. Relationship between the age of human erythrocytes and their osmotic resistance: a basis for separating old and young erythrocytes. *J. Clin. Invest.* 37:1542–1548.

16. Akeson, S. P., and H. C. Mel. 1983. Erythrocyte and ghost resistivity and voltage-dependent apparent size. *Biophys. J.* 44:397–403.

17. Richieri, G. V., S. P. Akeson, and H. C. Mel. 1985. Measurement of biophysical properties of red blood cells by resistive pulse spectroscopy: volume, shape, surface area, and deformability. *J. Biochem. Biophys. Methods.* 11:117–131.

18. Akeson, S. P., and H. C. Mel. 1982. Osmotic hemolysis and fragility.

A new model based on membrane disruption, and a potential clinical test. *Biochim. Biophys. Acta.* 718:201–211.

19. Nash, G. B., C. S. Johnson, and H. J. Meiselman. 1984. Mechanical properties of oxygenated red blood cells in sickle cell (HbSS) disease. *Blood.* 63:73–82.

20. Massaldi, H. A., A. Fuchs, and C. H. Borzi. 1983. The dynamics of the stress stage of osmotic haemolysis. *J. Biomech.* 16:103–107.

21. Savitz, D., V. W. Sidel, and A. K. Solomon. 1964. Osmotic properties of human red cells. *J. Gen. Physiol.* 48:79–85.

22. Evans, E., and Y. C. Fung. 1972. Improved measurement of the erythrocyte geometry. *Microvasc. Res.* 4:335–339.

23. Richieri, G. V., and H. C. Mel. 1985. Temperature effects on osmotic fragility, and the erythrocyte membrane. *Biochim. Biophys. Acta.* 813:41–50.

24. Richieri, G. 1984. Responses of red blood cell–membrane systems: temperature and calcium effects on volume, deformability, and osmotic fragility as studied by resistive pulse spectroscopy. Ph.D. thesis. University of California, Berkeley, CA. 171 pp.

25. Massaldi, H. A. 1984. The physicochemical mechanism of mediated transport. II. Osmotic and isosmotic volume flow. *J. Theor. Biol.* 110:35–55.

26. Macey, R. I. 1978. Water transport mechanisms. *In* Physiology of Membrane Disorders. T. E. Andreoli, J. E. Hoffman, and D. D. Fanestil, editors. Plenum Press, New York.

27. Massaldi, H. A., and C. H. Borzi. 1984. The physicochemical mechanism of mediated transport. I. Facilitated diffusion. *J. Theor. Biol.* 106:537–557.